



HAL
open science

Joint Localization and Information Transfer for RIS Aided Full-Duplex Systems

Zhichao Shao, Xiaojun Yuan, Wei Zhang, Marco Di Renzo

► **To cite this version:**

Zhichao Shao, Xiaojun Yuan, Wei Zhang, Marco Di Renzo. Joint Localization and Information Transfer for RIS Aided Full-Duplex Systems. GLOBECOM 2022 - 2022 IEEE Global Communications Conference, Dec 2022, Rio de Janeiro, Brazil. pp.3253-3258, 10.1109/GLOBECOM48099.2022.10001508 . hal-04262695

HAL Id: hal-04262695

<https://hal.science/hal-04262695v1>

Submitted on 27 Oct 2023

HAL is a multi-disciplinary open access archive for the deposit and dissemination of scientific research documents, whether they are published or not. The documents may come from teaching and research institutions in France or abroad, or from public or private research centers.

L'archive ouverte pluridisciplinaire **HAL**, est destinée au dépôt et à la diffusion de documents scientifiques de niveau recherche, publiés ou non, émanant des établissements d'enseignement et de recherche français ou étrangers, des laboratoires publics ou privés.

Joint Localization and Information Transfer for RIS Aided Full-Duplex Systems

Zhichao Shao[†], Xiaojun Yuan[†], Wei Zhang[‡], Marco Di Renzo[‡]

[†] Yangtze Delta Region Institute, University of Electronic Science and Technology of China, Huzhou, China

[†] National Key Lab. of Sci. and Tech. on Commun., Uni. of Electronic Sci. and Tech. of China, Chengdu, China

[‡] School of Electrical Engineering and Telecommunications, University of New South Wales, Sydney, Australia

[‡] Université Paris-Saclay, CNRS, CentraleSupélec, Laboratoire des Signaux et Systèmes, Paris, France

Email: {zhichao.shao, xjyuan}@uestc.edu.cn, w.zhang@unsw.edu.au, marco.direnzo@universite-paris-saclay.fr

Abstract—In this work, we investigate a reconfigurable intelligent surface (RIS) aided integrated sensing and communication (ISAC) scenario, where a base station (BS) communicates with multiple devices in a full-duplex mode, and senses the positions of these devices simultaneously. An RIS is assumed to be mounted on each device to enhance the reflected echoes. Meanwhile, the information of each device is passively transferred to the BS via reflection modulation. We aim to tackle the problem of joint localization and information retrieval at the BS. A grid based parametric model is constructed and the joint estimation problem is formulated as a compressive sensing (CS) problem. Moreover, an expectation-maximization (EM) algorithm is applied for tuning the grid parameters to mitigate the model mismatch problem. Finally, we analyze the efficacy of various CS algorithms through the Bayesian Cramér-Rao bound (BCRB). Numerical results demonstrate the feasibility of the proposed scenario and the superior performance of the proposed EM-tuning method.

Index Terms—ISAC, RIS, full-duplex system, compressive sensing, Bayesian Cramér-Rao bound

I. INTRODUCTION

Reconfigurable intelligent surface (RIS) has been envisioned as a promising next-generation wireless communication technology that is able to artificially tune wireless propagation channels [1]. An RIS consists of a large number of software-controlled meta-atoms with adjustable phase shifts to reflect incident electromagnetic waves towards desired directions, thereby significantly enhancing the communication quality. Moreover, an RIS, as a large passive antenna array, generally has remarkable capabilities to sense the environments, which has motivated research activities towards the integration of sensing and communications in RIS aided systems [2], [3]. For example, the authors of [2] employed one RIS for both sensing and communication where the direct path between the dual function radar and communication base station (BS) and the target exists. The goal was to maximize the radar signal-to-interference-plus-noise ratio (SINR) under the communication SINR constraint. The authors of [3] proposed an RIS that is adaptively partitioned into two parts for communication and localization, respectively, when no direct path exists.

In this work, we propose a new RIS-aided integrated sensing and communication (ISAC) scenario, where a BS not only communicates with multiple devices (such as vehicles) in full-

duplex, but also senses the positions of these devices simultaneously. We assume that an RIS is mounted on each device to enhance the echoes reflected by the device. Meanwhile, the information of each device is passively transferred to the BS via reflection modulation [4], [5], in which the information is encoded into the phase adjustments of RIS meta-atoms. The proposed ISAC scenario is advantageous in two aspects. First, the communication system is full-duplex in frequency and time, where the information delivered by the BS can be received by the devices using conventional receivers, and, at the same time/frequency slot, the information of the devices is passively delivered to the BS via reflection modulation thanks to the RISs. Second, the devices are “green” since they do not emit any electromagnetic signals during the whole process.

We consider a multiple-input multiple-output (MIMO) orthogonal frequency division multiplexing (OFDM) full-duplex system, and focus on the receiver design of the BS to jointly locating the positions of the devices and retrieving the information passively transferred by the RISs. We establish a grid-based parametric system model, and formulate the joint estimation problem as a compressive sensing (CS) problem by exploiting the sparsity on the considered parameter grid. Various CS algorithms [6]–[8] can be used to solve the problem. Moreover, an expectation-maximization (EM) algorithm is applied for tuning the grid parameters and mitigating the model mismatch problem. The Bayesian Cramér-Rao bound (BCRB) is also derived as a fundamental performance limit to evaluate the efficacy of various recovery algorithms. Numerical results demonstrate the feasibility of the proposed scenario, as well as the superior performance of the proposed EM-tuning method.

II. SYSTEM DESCRIPTION

A. RIS Aided Full-Duplex System

In the considered MIMO-OFDM full-duplex system, a BS with N_t transmit and N_r receive antennas communicates with multiple devices, each equipped with an RIS with L reflecting elements and a conventional receiver. The antenna and the element spacing is $\frac{\lambda}{2}$, where λ is the wavelength. The OFDM system has N orthogonal subcarriers, and the frequency spacing of adjacent subcarriers is $\Delta f = 1/T$, where T denotes the duration of one OFDM symbol. At the beginning of each OFDM symbol, a cyclic prefix (CP) of

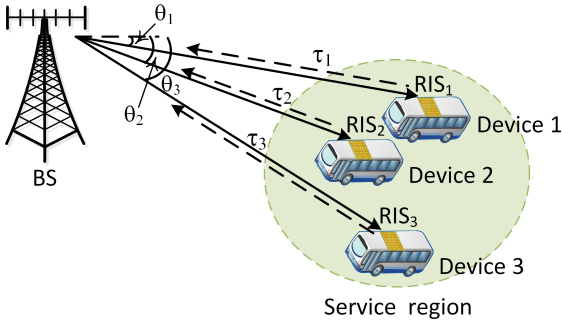


Fig. 1: An RIS-aided full-duplex system.

length T_{cp} is inserted to prevent the intersymbol interference, and the duration of each OFDM block is $T_b = T + T_{cp}$. The transmission protocol in Fig. 1 is described as follows. The BS first broadcasts the OFDM signal towards a given region by applying beamforming. The devices in the considered region receive the transmitted signal and recover it by using traditional signal processing techniques¹. Meanwhile, the RIS deployed on each device uses reflection modulation on the incident electromagnetic wave, and reflects it back to the BS. Unlike the incident wave, the reflected wave contains new information data that is sent from the RIS to the BS. Finally, the BS jointly estimates the positions and retrieves the information data of the devices from the received echos.

The transmitted signal in the m -th OFDM block at the BS is given by

$$\mathbf{x}_m(t) = \sum_{n=0}^{N-1} \mathbf{x}_m[n] e^{j2\pi n \Delta f t} \xi(t - mT_b), mT_b \leq t \leq (m+1)T_b, \quad (1)$$

where $\mathbf{x}_m[n] = [x_{m,1}[n], \dots, x_{m,N_t}[n]]^T \in \mathbb{C}^{N_t \times 1}$ contains the transmitted symbols at the n -th subcarrier in the m -th block;

$$\xi(t) = \begin{cases} 1, & t \in [0, T_b], \\ 0, & \text{otherwise.} \end{cases} \quad (2)$$

We assume that the line of sight (LOS) path exists and dominates the channel between the BS and each device. In fact, the considered application is different from conventional RIS-aided networks, where the RISs are utilized to create reliable virtual non-LOS paths. In the considered case study, the RISs are utilized to establish backscattered signals for transmitting data to the BS in a passive manner. We model the signal reflected by each device as a multipath characterized by an angle of propagation, a delay and a Doppler shift. We assume that there are K devices in the considered area. The delay and Doppler of the k -th path are denoted by τ_k and ν_k , respectively. Moreover, since the BS transmits and receives signals at the same time-frequency slot, the interference between the transmit and receive antennas needs to be considered while modeling the echos from the devices. In this work, we assume that the receive antennas are carefully isolated from the

¹We omit the details here since the receiver design at the device is not the focus of this paper.

transmit antennas so that the self-interference can be ignored [9]. The echos received at the BS are contaminated by an additive noise $\mathbf{w}_m(t) \in \mathbb{C}^{N_r \times 1}$ as

$$\mathbf{y}_m(t) = \sum_{k=0}^{K-1} \beta_k e^{j2\pi\nu_k t} \mathbf{H}_{UL,k} \mathbf{\Lambda}_k \mathbf{H}_{DL,k} \mathbf{x}_m(t - \tau_k) + \mathbf{w}_m(t), \quad (3)$$

where β_k is the round-trip fading coefficient accounting for the path attenuation from the BS to the k -th device and from the k -th device back to the BS; $\mathbf{\Lambda}_k = \text{diag}\{[e^{j\theta_{k,1,1}}, \dots, e^{j\theta_{k,N_x,N_y}}]\} \in \mathbb{C}^{L \times L}$ is a diagonal matrix whose diagonal elements are the phase shifts $\{\theta_{k,i,j}\}$ applied by the k -th RIS; $\mathbf{H}_{UL,k} \in \mathbb{C}^{N_r \times L}$ and $\mathbf{H}_{DL,k} \in \mathbb{C}^{L \times N_t}$ are the uplink and downlink channel matrices between the BS and the k -th device, respectively, given by

$$\mathbf{H}_{DL,k} = \mathbf{a}_{RIS}(\phi_{i,k}, \gamma_{i,k}) \mathbf{a}_{BS}(\vartheta_k)^H \quad (4)$$

$$\mathbf{H}_{UL,k} = \mathbf{b}_{BS}(-\vartheta_k) \mathbf{a}_{RIS}(\phi_{r,k}, \gamma_{r,k})^H, \quad (5)$$

where \mathbf{a}_{RIS} , \mathbf{a}_{BS} and \mathbf{b}_{BS} are the steering vectors defined in what follows. We assume that the elements of each RIS are arranged in a uniform rectangular array whose size is $N_x \times N_y$, where N_x and N_y are the columns and rows, respectively. $(\phi_{i,k}, \gamma_{i,k})$ and $(\phi_{r,k}, \gamma_{r,k})$ are the elevation and azimuth angles of arrival (AoA) and angles of departure (AoD) at the k -th RIS, respectively. The steering vector $\mathbf{a}_{RIS}(\phi_{i/r,k}, \gamma_{i/r,k}) \in \mathbb{C}^{L \times 1}$ is defined as

$$\mathbf{a}_{RIS}(\phi_{i/r,k}, \gamma_{i/r,k}) = \mathbf{a}_x(\phi_{i/r,k}, \gamma_{i/r,k}) \otimes \mathbf{a}_y(\phi_{i/r,k}, \gamma_{i/r,k}), \quad (6)$$

where \otimes denotes the Kronecker product; $\mathbf{a}_x(\phi_{i/r,k}, \gamma_{i/r,k}) \in \mathbb{C}^{N_x \times 1}$ and $\mathbf{a}_y(\phi_{i/r,k}, \gamma_{i/r,k}) \in \mathbb{C}^{N_y \times 1}$ are given as

$$\mathbf{a}_x(\phi_{i/r,k}, \gamma_{i/r,k}) = \frac{1}{\sqrt{N_x}} [1, \dots, e^{j\pi(N_x-1) \sin(\phi_{i/r,k}) \cos(\gamma_{i/r,k})}]^T \quad (7)$$

$$\mathbf{a}_y(\phi_{i/r,k}, \gamma_{i/r,k}) = \frac{1}{\sqrt{N_y}} [1, \dots, e^{j\pi(N_y-1) \sin(\phi_{i/r,k}) \sin(\gamma_{i/r,k})}]^T. \quad (8)$$

Moreover, we assume that both the transmit and receive antennas at the BS are arranged in a uniform linear antenna array. ϑ_k is the angle of departure (AoD) to the k -th RIS from the BS. The steering vectors $\mathbf{a}_{BS}(\vartheta_k) \in \mathbb{C}^{N_t \times 1}$ and $\mathbf{b}_{BS}(\vartheta_k) \in \mathbb{C}^{N_r \times 1}$ are expressed as

$$\mathbf{a}_{BS}(\vartheta_k) = \frac{1}{\sqrt{N_t}} [1, e^{j\pi \sin(\vartheta_k)}, \dots, e^{j\pi(N_t-1) \sin(\vartheta_k)}]^T \quad (9)$$

$$\mathbf{b}_{BS}(\vartheta_k) = \frac{1}{\sqrt{N_r}} [1, e^{j\pi \sin(\vartheta_k)}, \dots, e^{j\pi(N_r-1) \sin(\vartheta_k)}]^T. \quad (10)$$

Since each RIS is designed to reflect the incident signal towards the opposite direction (i.e., the RIS operates as a retro-reflective metasurface for backscattering enhancement), the AoAs and the AoDs at the BS are opposite. Defining

$$\alpha_k = \beta_k \mathbf{a}_{RIS}(\phi_{r,k}, \gamma_{r,k})^H \mathbf{\Lambda}_k \mathbf{a}_{RIS}(\phi_{i,k}, \gamma_{i,k}), \quad (11)$$

we can rewrite (3) as

$$\mathbf{y}_m(t) = \sum_{k=0}^{K-1} \alpha_k e^{j2\pi\nu_k t} \mathbf{H}(\vartheta_k) \mathbf{x}_m(t - \tau_k) + \mathbf{w}_m(t), \quad (12)$$

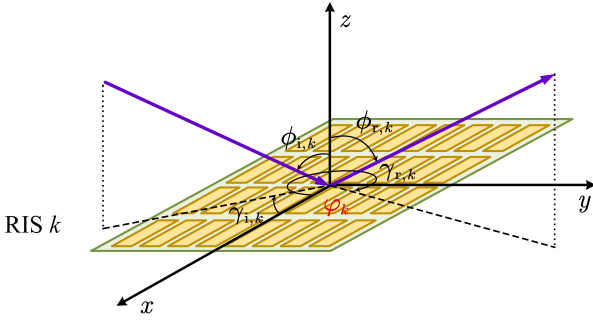


Fig. 2: An illustration of the generalized Snell's law.

where $\mathbf{H}(\vartheta_k) = \mathbf{b}_{\text{BS}}(-\vartheta_k)\mathbf{a}_{\text{BS}}(\vartheta_k)^H \in \mathbb{C}^{N_r \times N_t}$. For the m -th block, the demodulated signal at the n -th subcarrier is

$$\mathbf{y}_m[n] = \frac{1}{T} \int_{mT_b + T_{cp}}^{(m+1)T_b} e^{-j2\pi n \Delta f t} \mathbf{y}_m(t) dt. \quad (13)$$

Plugging (1) and (12) into (13), we have

$$\mathbf{y}_m[n] = \sum_{k=0}^{K-1} \alpha_k c_k e^{-j2\pi n \Delta f \tau_k} \mathbf{H}(\vartheta_k) \mathbf{x}_m[n] + \mathbf{w}_m[n], \quad (14)$$

where

$$c_k = \frac{1}{T} \int_{mT_b + T_{cp}}^{(m+1)T_b} e^{j2\pi \nu_k t} dt \quad (15)$$

$$\mathbf{w}_m[n] = \frac{1}{T} \int_{mT_b + T_{cp}}^{(m+1)T_b} e^{-j2\pi n \Delta f t} \mathbf{w}_m(t) dt \quad (16)$$

with $\mathbf{w}_m[n] \in \mathbb{C}^{N_r \times 1} \sim \mathcal{CN}(\mathbf{0}, \sigma^2 \mathbf{I}_{N_r})$.

B. Passive Beamforming and Information Transfer of RIS

We first illustrate an anomalous reflection scenario shown in Fig. 2, where $\phi_i \in [-\frac{\pi}{2}, \frac{\pi}{2}]$ and $\gamma_i \in [0, 2\pi]$ are the elevation and the azimuth angle of the incident wave, respectively, $\phi_r \in [-\frac{\pi}{2}, \frac{\pi}{2}]$ and $\gamma_r \in [0, 2\pi]$ are the elevation and the azimuth angle of the reflected wave, respectively. According to the generalized Snell's law [10], to reflect an incident plane wave into a desired direction, breaking the specular reflection law ($\phi_r = \phi_i$ and $\gamma_r = \gamma_i + \pi$), the reflection phase of each element should depend linearly on the corresponding coordinate of both the x- and y-axes. Given the reference phase of the origin of the coordinates φ_k , the phase of the (i, j) -th element $\theta_{k,i,j}$ of the k -th RIS is obtained by [11], the phase shift of the (i, j) -th element $\theta_{k,i,j}$ at the k -th RIS is

$$\theta_{k,i,j} = \pi(i-1)q_{x,k} + \pi(j-1)q_{y,k} + \varphi_k, \quad (17)$$

where $q_{x,k}$ and $q_{y,k}$ denote the phase gradients of the x- and y-axes, calculated as

$$\begin{bmatrix} q_{x,k} \\ q_{y,k} \end{bmatrix} = \begin{bmatrix} \sin(\phi_{r,k}) \cos(\gamma_{r,k}) + \sin(\phi_{i,k}) \cos(\gamma_{i,k}) \\ \sin(\phi_{r,k}) \sin(\gamma_{r,k}) + \sin(\phi_{i,k}) \sin(\gamma_{i,k}) \end{bmatrix}. \quad (18)$$

Equation (18) reveals that the anomalous reflection from arbitrary angles $(\phi_{i,k}, \gamma_{i,k})$ to arbitrary angles $(\phi_{r,k}, \gamma_{r,k})$ can be achieved by setting $q_{x,k}$ and $q_{y,k}$ accordingly. Besides, another degree of freedom provided in (17) is the reference

phase φ_k of the k -th RIS, which determines the wavefront phase of the reflected beam. Especially, for the scenario of retro-reflection ($\phi_{r,k} = -\phi_{i,k}$ and $\gamma_{r,k} = \gamma_{i,k}$), we have

$$\begin{bmatrix} q_{x,k} \\ q_{y,k} \end{bmatrix} = \begin{bmatrix} -2 \sin(\phi_k) \cos(\gamma_k) \\ -2 \sin(\phi_k) \sin(\gamma_k) \end{bmatrix} \quad (19)$$

In practice, the angles $\phi_{i,k}$ and $\gamma_{i,k}$ can be estimated through sensors deployed at the k -th device, e.g., by using the MUSIC algorithm [12]. Plugging (17) into (11), we have

$$\begin{aligned} \alpha_k &= \frac{\beta_k}{L} \sum_{i=1}^{N_x} \sum_{j=1}^{N_y} e^{j2\pi(i-1) \sin(\phi_{r,k}) \cos(\gamma_{r,k})} e^{j\theta_{k,i,j}} \\ &\quad \times e^{j2\pi(j-1) \sin(\phi_{i,k}) \sin(\gamma_{i,k})} \\ &= \beta_k e^{j\varphi_k}, \end{aligned} \quad (20a) \quad (20b)$$

where φ_k can be easily controlled by the RIS. This motivates us to use reflection modulation on the incident wave [13]. The reflected wave, or more specifically φ_k , can be utilized to passively transmit new information that is generated at the device and needs to be sent to the BS.

Note that $\mathbf{x}_m[n]$ is the self-information known by the BS. Then, the problem we are interested in consists of jointly estimating the unknown parameters ϑ_k , τ_k , ν_k and φ_k from the noisy observations $\{\mathbf{y}_m[n]\}$ in (14).

III. JOINT LOCALIZATION AND INFORMATION RECOVERY

In this section, we first introduce the grid-based parametric model to formulate the problem stated in the previous section, and then discuss CS algorithms to solve it.

A. Parametric Grid Model

The angle, delay and Doppler domains (location parameters) are uniformly sampled into a set of Q , U and V discrete values, defined as

$$\vartheta = [\vartheta_0, \dots, \vartheta_{Q-1}]^T, \quad \vartheta_q \in [\vartheta_{\min}, \vartheta_{\max}] \quad (21a)$$

$$\tau = [\tau_0, \dots, \tau_{U-1}]^T, \quad \tau_u \in [\tau_{\min}, \tau_{\max}] \quad (21b)$$

$$\nu = [\nu_0, \dots, \nu_{V-1}]^T, \quad \nu_v \in [\nu_{\min}, \nu_{\max}]. \quad (21c)$$

Based on the above discretized points, (14) is rewritten as

$$\begin{aligned} \mathbf{y}_m[n] &= \sum_{v=0}^{V-1} \sum_{u=0}^{U-1} \sum_{q=0}^{Q-1} c_v e^{-j2\pi n \Delta f \tau_u} \mathbf{H}(\vartheta_q) \mathbf{x}_m[n] \zeta_{v,u,q} + \mathbf{w}_m[n] \\ &= \mathbf{Z}_m[n] \boldsymbol{\zeta} + \mathbf{w}_m[n] \end{aligned} \quad (22)$$

with

$$\mathbf{Z}_m[n] = \mathbf{c} \otimes (e^{-j2\pi n \Delta f \tau})^T \otimes \mathbf{H}(\boldsymbol{\vartheta}) (\mathbf{I}_Q \otimes \mathbf{x}_m[n]), \quad (23)$$

where $\mathbf{c} = [c_0, \dots, c_{V-1}]^T \in \mathbb{C}^{V \times 1}$, $e^{-j2\pi n \Delta f \tau} = [e^{-j2\pi n \Delta f \tau_0}, \dots, e^{-j2\pi n \Delta f \tau_{U-1}}]^T \in \mathbb{C}^{U \times 1}$, $\mathbf{H}(\boldsymbol{\vartheta}) = [\mathbf{H}(\vartheta_0), \dots, \mathbf{H}(\vartheta_{Q-1})] \in \mathbb{C}^{N_r \times Q N_t}$. $\boldsymbol{\zeta} = [\zeta_{1,1,1}, \dots, \zeta_{1,1,Q}, \zeta_{1,2,1}, \dots, \zeta_{1,U,Q}, \zeta_{2,1,1}, \dots, \zeta_{V,U,Q}]^T \in \mathbb{C}^{V U Q \times 1}$, where $\zeta_{v,u,q}$ denotes the α of a possible device at the v -th, u -th and q -th grid point in (21). Since there are only K devices in the considered region, $\boldsymbol{\zeta}$ is a sparse

vector, where the non-zero elements represent the $\{\alpha_k\}$ of the devices.

Collecting the received signals on N subcarriers, we obtain

$$\mathbf{y}_m = [\mathbf{y}_m[1]^T, \dots, \mathbf{y}_m[N]^T]^T = \mathbf{Z}_m \boldsymbol{\zeta} + \mathbf{w}_m, \quad (24)$$

where $\mathbf{Z}_m = [\mathbf{Z}_m[1]^T, \dots, \mathbf{Z}_m[N]^T]^T \in \mathbb{C}^{N_r N \times VUQ}$ and $\mathbf{w}_m = [\mathbf{w}_m[1]^T, \dots, \mathbf{w}_m[N]^T]^T \in \mathbb{C}^{N_r N \times 1}$. Moreover, by stacking all the demodulated symbols in M OFDM blocks into a column vector $\mathbf{y} \in \mathbb{C}^{N_r NM \times 1}$, we have

$$\mathbf{y} = [\mathbf{y}_1^T, \dots, \mathbf{y}_M^T]^T = \mathbf{Z} \boldsymbol{\zeta} + \mathbf{w}, \quad (25)$$

where $\mathbf{Z} = [\mathbf{Z}_1^T, \dots, \mathbf{Z}_M^T]^T \in \mathbb{C}^{N_r NM \times VUQ}$ and $\mathbf{w} = [\mathbf{w}_1^T, \dots, \mathbf{w}_M^T]^T \in \mathbb{C}^{N_r NM \times 1}$.

With the knowledge of the transmitted symbols $\mathbf{x}_m[n]$ and the grids in (21), the matrix \mathbf{Z} is known by the BS. The estimation problem is converted into the problem of estimating $\boldsymbol{\zeta}$ based on \mathbf{y} in (25). By noting the sparsity of $\boldsymbol{\zeta}$, it can be recovered by using CS techniques.

B. Algorithm Design

In the following, we solve $\boldsymbol{\zeta}$ given \mathbf{y} in (25) for two scenarios, namely, the on-grid and off-grid models.

1) *On-Grid Model*: In this case, the localization parameters to be estimated are assumed to be placed on the grid specified in (21). By leveraging the sparsity of $\boldsymbol{\zeta}$, several algorithms can be used to solve (25), such as the orthogonal matching pursuit (OMP) [6] and the sparse Bayesian learning (SBL) [7] method. However, OMP has low estimation accuracy, and SBL involves high computational complexity due to the need of matrix inversion. In this work, we apply the Bernoulli-Gaussian generalized approximate message passing (BG-GAMP) [8] algorithm for solving (25), which can offer a high accuracy and low complexity.

Since each device is independent and identically distributed in the considered region, the distribution $p(\boldsymbol{\zeta})$ is modeled as Bernoulli-Gaussian, i.e.,

$$p(\boldsymbol{\zeta}) = \prod_i^{VUQ} ((1 - \rho)\delta(\zeta_i) + \rho\mathcal{CN}(\zeta_i; \bar{\alpha}, v_\alpha)), \quad (26)$$

where $\rho = \frac{K}{VUQ}$ is the sparsity of $\boldsymbol{\zeta}$; $\delta(\cdot)$ is the Dirac delta function; $p(\alpha_k)$ is approximated with a Gaussian distribution with mean $\bar{\alpha}$ and variance v_α for simplification². The posterior probability $p(\boldsymbol{\zeta}|\mathbf{y})$ is calculated as

$$p(\boldsymbol{\zeta}|\mathbf{y}) = \frac{1}{p(\mathbf{y})} p(\mathbf{y}|\boldsymbol{\zeta}) p(\boldsymbol{\zeta}), \quad (27)$$

where $p(\mathbf{y}|\boldsymbol{\zeta}) \sim \mathcal{CN}(\mathbf{y}; \mathbf{Z}\boldsymbol{\zeta}, \sigma^2 \mathbf{I}_{N_r NM})$.

²In practice, the fading coefficient β_k in α_k is the multiplication of two fading coefficients correspondingly to the forward and backward (reflected) links. Since there is no prior information about the two fading coefficients, we treat the multiplication as an unknown variable, whose distribution is assumed to be Gaussian.

2) *Off-Grid Model*: It is worth noting that the true localization parameters may not be in the given grids resulting in a model mismatch. To address this issue, we treat $\boldsymbol{\vartheta}$, $\boldsymbol{\tau}$ and $\boldsymbol{\nu}$ in \mathbf{Z} as unknown parameters and consider learning these parameters to improve the BG-GAMP performance.

Let $\boldsymbol{\omega} = \{\boldsymbol{\vartheta}, \boldsymbol{\tau}, \boldsymbol{\nu}\}$. The parameter set $\boldsymbol{\omega}$ is updated through the EM method. The EM method is an iterative process with each iteration consisting two steps, namely, the E-step and the M-step. Denote by $\boldsymbol{\omega}_i$ the parameter set $\boldsymbol{\omega}$ in the i -th iteration. The E-step calculates the expectation of the log-likelihood evaluated using the current estimate as

$$\begin{aligned} \mathcal{Q}(\boldsymbol{\omega}, \boldsymbol{\omega}_i) &= E_{p(\boldsymbol{\zeta}|\mathbf{y}, \boldsymbol{\omega}_i)} \{\ln p(\mathbf{y}, \boldsymbol{\zeta}|\boldsymbol{\omega})\} \\ &= \int \ln p(\mathbf{y}|\boldsymbol{\omega}, \boldsymbol{\zeta}) p(\boldsymbol{\zeta}|\mathbf{y}, \boldsymbol{\omega}_i) d\boldsymbol{\zeta} + \int \ln p(\boldsymbol{\zeta}|\boldsymbol{\omega}) p(\boldsymbol{\zeta}|\mathbf{y}, \boldsymbol{\omega}_i) d\boldsymbol{\zeta}. \end{aligned} \quad (28)$$

The M-step is to maximize (28), that is

$$\max_{\boldsymbol{\omega}} \int \ln p(\mathbf{y}|\boldsymbol{\omega}, \boldsymbol{\zeta}) p(\boldsymbol{\zeta}|\mathbf{y}, \boldsymbol{\omega}_i) d\boldsymbol{\zeta}, \quad (29)$$

where the last term in (28) is dropped since it is irrelevant to $\boldsymbol{\omega}$ by noting $p(\boldsymbol{\zeta}|\boldsymbol{\omega}) = p(\boldsymbol{\zeta})$. Plugging (27) into (29) and ignoring the terms independent of $\boldsymbol{\omega}$, we have

$$\max_{\boldsymbol{\omega}} \mathcal{G}(\boldsymbol{\omega}, \boldsymbol{\omega}_i) = 2\mathcal{R}\{\mathbf{y}^H \mathbf{Z}(\boldsymbol{\omega}) \bar{\boldsymbol{\zeta}}_i\} - Tr\{\mathbf{Z}(\boldsymbol{\omega})^H \mathbf{Z}(\boldsymbol{\omega}) \boldsymbol{\Omega}_i\}, \quad (30)$$

where $\boldsymbol{\Omega}_i = \mathbf{V}_{\boldsymbol{\zeta}_i} + \bar{\boldsymbol{\zeta}}_i \bar{\boldsymbol{\zeta}}_i^H$, $\bar{\boldsymbol{\zeta}}_i$ and $\mathbf{V}_{\boldsymbol{\zeta}_i}$ are the posterior mean and variance calculated in (27) based on $\boldsymbol{\omega} = \boldsymbol{\omega}_i$; $\mathcal{R}\{\cdot\}$ represents the real part; $Tr\{\cdot\}$ denotes the trace operation.

In practice, it is not easy to obtain a closed-form solution to (30) since the problem is highly non-linear in $\boldsymbol{\vartheta}$, $\boldsymbol{\tau}$ and $\boldsymbol{\nu}$. Therefore, we propose the gradient descent method to iteratively maximize $\mathcal{G}(\boldsymbol{\omega}, \boldsymbol{\omega}_i)$. The update rule is

$$\boldsymbol{\omega}_{i+1} = \boldsymbol{\omega}_i + \epsilon \nabla \mathcal{G}(\boldsymbol{\omega}, \boldsymbol{\omega}_i), \quad (31)$$

where ϵ is an appropriate stepsize, and

$$\begin{aligned} \nabla \mathcal{G}(\boldsymbol{\omega}, \boldsymbol{\omega}_i) &= 2\mathcal{R} \left\{ \mathbf{y}^H \frac{\partial \mathbf{Z}(\boldsymbol{\omega})}{\partial \boldsymbol{\omega}} \bar{\boldsymbol{\zeta}}_i \right\} \\ &\quad - Tr \left\{ \left(\frac{\partial \mathbf{Z}(\boldsymbol{\omega})^H}{\partial \boldsymbol{\omega}} \mathbf{Z}(\boldsymbol{\omega}) + \mathbf{Z}(\boldsymbol{\omega})^H \frac{\partial \mathbf{Z}(\boldsymbol{\omega})}{\partial \boldsymbol{\omega}} \right) \boldsymbol{\Omega}_i \right\}. \end{aligned} \quad (32)$$

From (23), the derivatives with respect to $\boldsymbol{\vartheta}$, $\boldsymbol{\tau}$ and $\boldsymbol{\nu}$ are given by

$$\frac{\partial \mathbf{Z}_m[n]}{\partial \boldsymbol{\vartheta}} = \mathbf{c} \otimes (e^{-j2\pi n \Delta f \boldsymbol{\tau}})^T \otimes \frac{\partial \mathbf{H}(\boldsymbol{\vartheta})}{\partial \boldsymbol{\vartheta}} (\mathbf{I}_Q \otimes \mathbf{x}_m[n]), \quad (33a)$$

$$\frac{\partial \mathbf{Z}_m[n]}{\partial \boldsymbol{\tau}} = \mathbf{c} \otimes \frac{\partial (e^{-j2\pi n \Delta f \boldsymbol{\tau}})^T}{\partial \boldsymbol{\tau}} \otimes \mathbf{H}(\boldsymbol{\vartheta}) (\mathbf{I}_Q \otimes \mathbf{x}_m[n]), \quad (33b)$$

$$\frac{\partial \mathbf{Z}_m[n]}{\partial \boldsymbol{\nu}} = \frac{\partial \mathbf{c}}{\partial \boldsymbol{\nu}} \otimes (e^{-j2\pi n \Delta f \boldsymbol{\tau}})^T \otimes \mathbf{H}(\boldsymbol{\vartheta}) (\mathbf{I}_Q \otimes \mathbf{x}_m[n]). \quad (33c)$$

The overall procedure is summarized in Algorithm 1.

Algorithm 1 EM-BG-GAMP

- 1: **Input:** \mathbf{y} , \mathbf{Z} , $p(\zeta)$
 - 2: **while** The stopping criterion is not met **do**
 - 3: Use the BG-GAMP [8] to obtain $\tilde{\zeta}_i$ and $\mathbf{V}_{\tilde{\zeta}_i}$.
 - 4: Fix $\boldsymbol{\nu}$, $\boldsymbol{\tau}$, and maximize (30) with respect to $\boldsymbol{\vartheta}$ through gradient descent (31) to obtain $\boldsymbol{\vartheta}_{i+1}$.
 - 5: Fix $\boldsymbol{\nu}$, $\boldsymbol{\vartheta}$, and maximize (30) with respect to $\boldsymbol{\tau}$ through gradient descent (31) to obtain $\boldsymbol{\tau}_{i+1}$.
 - 6: Fix $\boldsymbol{\tau}$, $\boldsymbol{\vartheta}$, and maximize (30) with respect to $\boldsymbol{\nu}$ through gradient descent (31) to obtain $\boldsymbol{\nu}_{i+1}$.
 - 7: Generate new \mathbf{Z} based on $\boldsymbol{\vartheta}_{i+1}$, $\boldsymbol{\tau}_{i+1}$ and $\boldsymbol{\nu}_{i+1}$.
 - 8: **end while**
 - 9: **Output:** $\hat{\boldsymbol{\vartheta}}$, $\hat{\boldsymbol{\tau}}$, $\hat{\boldsymbol{\nu}}$ and $\hat{\zeta}$
-

IV. BAYESIAN CRAMÉR-RAO BOUND

We now develop a mean square error lower-bound of the considered estimation problem by assuming that the support of ζ is known. Then, the signal model in (25) reduces to

$$\mathbf{y} = \mathbf{Z}_{\text{real}} \boldsymbol{\zeta}_{\text{real}} + \mathbf{w}, \quad (34)$$

where $\mathbf{Z}_{\text{real}} \in \mathbb{C}^{N_r N M \times K}$ is similar to \mathbf{Z} but it is constructed by the angles $\boldsymbol{\vartheta}_{\text{real}} = [\vartheta_1, \dots, \vartheta_K]^T \in \mathbb{R}^{K \times 1}$, delays $\boldsymbol{\tau}_{\text{real}} = [\tau_1, \dots, \tau_K]^T \in \mathbb{R}^{K \times 1}$ and Doppler shifts $\boldsymbol{\nu}_{\text{real}} = [\nu_1, \dots, \nu_K] \in \mathbb{R}^{K \times 1}$; $\boldsymbol{\zeta}_{\text{real}} = [\alpha_1, \dots, \alpha_K]^T \in \mathbb{C}^{K \times 1}$. Let $\boldsymbol{\kappa} = [\boldsymbol{\vartheta}_{\text{real}}^T, \boldsymbol{\tau}_{\text{real}}^T, \boldsymbol{\nu}_{\text{real}}^T, \boldsymbol{\zeta}_{\text{real}}^T]^T$ be the parameter vector. The Bayesian information matrix (BIM) [14] is defined as

$$[\mathbf{J}_{\mathbf{y}}(\boldsymbol{\kappa})]_{i,j} = [\mathbf{J}_{\mathbf{y}}^{\text{D}}(\boldsymbol{\kappa})]_{i,j} + [\mathbf{J}_{\mathbf{y}}^{\text{P}}(\boldsymbol{\kappa})]_{i,j}, \quad (35)$$

where

$$[\mathbf{J}_{\mathbf{y}}^{\text{D}}(\boldsymbol{\kappa})]_{i,j} = E_{\mathbf{y}|\boldsymbol{\kappa}} \left\{ \frac{\partial \ln p(\mathbf{y}|\boldsymbol{\kappa})}{\partial \kappa_i} \frac{\partial \ln p(\mathbf{y}|\boldsymbol{\kappa})}{\partial \kappa_j} \right\} \quad (36)$$

$$[\mathbf{J}_{\mathbf{y}}^{\text{P}}(\boldsymbol{\kappa})]_{i,j} = E_{\boldsymbol{\kappa}} \left\{ \frac{\partial \ln p(\boldsymbol{\kappa})}{\partial \kappa_i} \frac{\partial \ln p(\boldsymbol{\kappa})}{\partial \kappa_j} \right\} \quad (37)$$

with κ_i being the i -th element of $\boldsymbol{\kappa}$. Since $\mathbf{y} \sim \mathcal{CN}(\mathbf{Z}_{\text{real}} \boldsymbol{\zeta}_{\text{real}}, \sigma^2 \mathbf{I}_{N_r N M})$, (36) is calculated as

$$[\mathbf{J}_{\mathbf{y}}^{\text{D}}(\boldsymbol{\kappa})]_{i,j} = \frac{2}{\sigma^2} \mathcal{R} \left\{ \left(\frac{\partial (\mathbf{Z}_{\text{real}} \boldsymbol{\zeta}_{\text{real}})}{\partial \kappa_i} \right)^H \frac{\partial (\mathbf{Z}_{\text{real}} \boldsymbol{\zeta}_{\text{real}})}{\partial \kappa_j} \right\}, \quad (38)$$

where the derivatives are similar to (33) and their expressions are omitted here due to space limitation. Moreover, since $p(\boldsymbol{\zeta}_{\text{real}})$ in (26) needs to be *a priori* known in the BG-GAMP algorithm, the $\boldsymbol{\zeta}_{\text{real}}$ in (37) is calculated as

$$[\mathbf{J}_{\mathbf{y}}^{\text{P}}(\boldsymbol{\zeta}_{\text{real}})]_{i,j} = E_{\boldsymbol{\zeta}_{\text{real}}} \left\{ \frac{\partial \ln p(\boldsymbol{\zeta}_{\text{real}})}{\partial \zeta_{\text{real},i}} \frac{\partial \ln p(\boldsymbol{\zeta}_{\text{real}})}{\partial \zeta_{\text{real},j}} \right\} = \frac{2}{v_{\alpha}}. \quad (39)$$

Since $\boldsymbol{\vartheta}_{\text{real}}$, $\boldsymbol{\tau}_{\text{real}}$ and $\boldsymbol{\nu}_{\text{real}}$ are uniformly distributed in the corresponding ranges, $[\mathbf{J}_{\mathbf{y}}^{\text{P}}(\boldsymbol{\vartheta}_{\text{real}})]_{i,j}$, $[\mathbf{J}_{\mathbf{y}}^{\text{P}}(\boldsymbol{\tau}_{\text{real}})]_{i,j}$ and $[\mathbf{J}_{\mathbf{y}}^{\text{P}}(\boldsymbol{\nu}_{\text{real}})]_{i,j}$ are all zero. The BCRB³ for the estimation of $\boldsymbol{\kappa}$ is given by

$$\text{Var}\{\boldsymbol{\kappa}_i\} = [\mathbf{J}_{\mathbf{y}}^{-1}(\boldsymbol{\kappa})]_{i,i}, \quad (40)$$

³Compared to the CRB, which gives fundamental lower limits to the variance of any unbiased estimator, the BCRB is used for random variables and provides a lower bound on the variance of any estimator.

where $\text{Var}\{\cdot\}$ denotes the variance. Moreover, we note that

$$\mathbf{d}_{\text{real}} = \frac{c}{2} \boldsymbol{\tau}_{\text{real}}, \quad (41)$$

where $\mathbf{d}_{\text{real}} = [d_1, \dots, d_K]^T \in \mathbb{R}^{K \times 1}$ are the distances between the BS and the devices with c being the light speed. Thus, the BCRB for the estimation of \mathbf{d}_{real} is given by

$$\text{Var}\{d_{\text{real},i}\} = \frac{c^2}{4} \text{Var}\{\tau_{\text{real},i}\}. \quad (42)$$

Specifically, $\boldsymbol{\kappa}$ is reduced to $\boldsymbol{\zeta}_{\text{real}}$ in the on-grid system, since the localization parameters are constituted by the grid values in (21). The indices can be obtained through the positions of non-zero elements in $\boldsymbol{\zeta}$.

V. NUMERICAL RESULTS

The parameters used in the simulation are listed in Tab. I. The fading coefficient β_k is given by [15]

$$\beta_k = \eta_k \sqrt{G_t G_r G \frac{L^2 \lambda^4}{64\pi^3 d_k^4}} \quad (43)$$

with $\eta_k \sim \mathcal{CN}(0, 1)$, $G_t = 100$, $G_r = 100$ and $G = 1$ being the transmitter, receiver and RIS gains, respectively. Since the waveform propagates much faster than the devices' velocities, we make the approximation that the distances from the BS to the RIS and from the RIS to the BS are the same as d_k . The SNR is defined as $10 \log \frac{\|\mathbf{Z}_{\text{real}} \boldsymbol{\zeta}_{\text{real}}\|_2^2}{N_r N M \sigma^2}$. The mean and variance in (26) are

$$\bar{\alpha} = 0 \quad v_{\alpha} = \frac{P_{\min}^2 + P_{\min} P_{\max} + P_{\max}^2}{3} + \frac{(P_{\min} + P_{\max})^2}{4}, \quad (44)$$

where $P_{\max} = \sqrt{G_t G_r G \frac{L^2 \lambda^4}{64\pi^3 d_{\min}^4}}$, P_{\min} is similarly defined.

TABLE I: Global parameters

Parameters	Symbols	Values
Subcarrier spacing	Δf	15 kHz
CP duration	T_{cp}	16.67 μs
Number of subcarriers	N	16
Number of transmit antennas	N_t	16
Number of receive antennas	N_r	4
Range of angle	ϑ	$[-30^\circ, 30^\circ]$
Range of distance	d	[100 m, 120 m]
Range of Doppler frequency	ν	[-2 kHz, 2 kHz]
Number of reflecting elements on RIS	L	30 \times 30
Number of transmitted symbols	M	16

Fig. 4 shows the normalized mean square error (NMSE) of $\boldsymbol{\zeta}_{\text{real}}$ and the symbol error rate (SER) of the transmitted symbols $\{\alpha_k\}$ in the on-grid system. To further recover the modulated phase $\{\varphi_k\}$ in $\{\alpha_k\}$, the differential phase shift keying (DPSK) modulation is applied since $\{\beta_k\}$ change slowly and can be treated as constant values during multiple successive OFDM blocks. With the DPSK, the unknown phases caused by $\{\beta_k\}$ can be compensated. Considering differential quadrature phase shift keying (DQPSK) modulation as an example, the modulated phase $\{\varphi_k\}$ for the information bits transferred at the RIS are $\{e^{\pm \frac{\pi}{4}}, e^{\pm \frac{3\pi}{4}}\}$ and the transmitted symbols $\{\alpha_k\}$ belong to $\{\beta_k e^{\pm \frac{\pi}{4}}, \beta_k e^{\pm \frac{3\pi}{4}}\}$. The numbers of grid points in

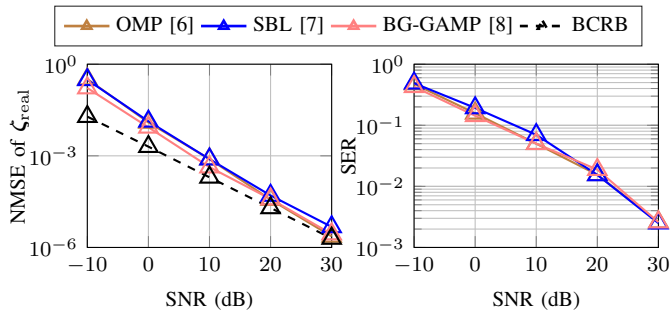


Fig. 4: On-grid system.

the angle, delay and Doppler domains are set as 10, 10 and 20, respectively, so that the resolutions $\Delta\omega$ in the corresponding domains are 3° , 13.3 ns and 200 Hz. The sparse vector ζ to be recovered is of length 2000, and contains 4 non-zero elements, i.e., there are $K = 4$ devices in the service region. In the on-grid system, the values of the localization parameters are taken over the grid in (21), and the indices can be obtained through the positions of non-zero elements in ζ . It is observed that all three algorithms have almost the same NMSE performance in the estimation of ζ and the same SER performance while recovering the information transmitted from the device.

Moreover, Fig. 5 shows the performance of parameter tuning with the EM algorithm in the off-grid system, where the localization parameters θ_{real} and τ_{real} are set as the values around the grid points within the range of $0.2\Delta\omega$. The relationship between \mathbf{d}_{real} and τ_{real} can be found in (41). The initial grids are the same with the on-grid system in (21). It can be seen that the EM method can effectively correct the model mismatches and improve the NMSE and SER performance. The proposed EM-BG-GAMP algorithm significantly outperforms the other baseline methods, especially at high SNR.

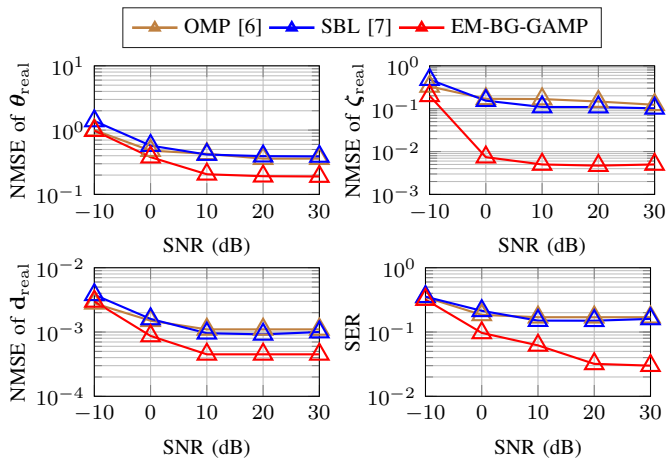


Fig. 5: Off-grid system.

VI. CONCLUSIONS

In this work, we have proposed a new RIS-aided ISAC scenario, where a BS communicates with multiple devices in full-duplex mode, and senses the positions of these devices simultaneously. A grid based parametric model was

constructed, and the joint estimation problem was formulated as a CS problem. Several CS algorithms were used to solve the problem. To tackle the issue of model mismatch, an EM algorithm was utilized for parameter tuning. Simulation results have shown the good performance of the proposed method.

ACKNOWLEDGMENT

This work was supported by the General Program of National Natural Science Foundation of China (No. 62071090) and the Sichuan Science and Technology Program (No. 2021YFH0014). The work of M. Di Renzo was supported in part by the European Commission through the H2020 ARIADNE project under grant agreement number 871464 and through the H2020 RISE-6G project under grant agreement number 101017011.

REFERENCES

- [1] M. Di Renzo, A. Zappone, M. Debbah, M.-S. Alouini, C. Yuen, J. de Rosny, and S. Tretyakov, "Smart radio environments empowered by reconfigurable intelligent surfaces: How it works, state of research, and the road ahead," *IEEE J. Sel. Areas Commun.*, vol. 38, no. 11, pp. 2450–2525, 2020.
- [2] Z.-M. Jiang, M. Rihan, P. Zhang, L. Huang, Q. Deng, J. Zhang, and E. M. Mohamed, "Intelligent reflecting surface aided dual-function radar and communication system," *IEEE Syst. J.*, Feb. 2021.
- [3] R. S. P. Sankar, B. Deepak, and S. P. Chepuri, "Joint communication and radar sensing with reconfigurable intelligent surfaces," *arXiv:2105.01966*, Sept. 2021.
- [4] W. Yan, X. Yuan, and X. Kuai, "Passive beamforming and information transfer via large intelligent surface," *IEEE Wireless Commun. Lett.*, vol. 9, no. 4, pp. 533–537, Dec. 2020.
- [5] W. Yan, X. Yuan, Z.-Q. He, and X. Kuai, "Passive beamforming and information transfer design for reconfigurable intelligent surfaces aided multiuser MIMO systems," *IEEE J. Sel. Areas Commun.*, vol. 38, no. 8, pp. 1793–1808, Jun. 2020.
- [6] J. A. Tropp and A. C. Gilbert, "Signal recovery from random measurements via orthogonal matching pursuit," *IEEE Trans. Inf. Theory*, vol. 53, no. 12, pp. 4655–4666, Mar. 2007.
- [7] M. E. Tipping, "Sparse bayesian learning and the relevance vector machine," *J. Mach. Learn. Res.*, pp. 211–244, Jan. 2001.
- [8] J. Vila and P. Schniter, "Expectation-maximization bernoulli-gaussian approximate message passing," in *the Forty Fifth Asilomar Conference on Signals, Systems and Computers*, Apr. 2011.
- [9] E. Everett, A. Sahai, and A. Sabharwal, "Passive self-interference suppression for full-duplex infrastructure nodes," *IEEE Trans. Wireless Commun.*, vol. 13, no. 2, pp. 680–694, Jan. 2014.
- [10] N. Yu *et al.*, "Light propagation with phase discontinuities: Generalized laws of reflection and refraction," *Science*, vol. 334, no. 6054, pp. 333–337, 2011.
- [11] C. Cai, X. Yuan, W. Yan, Z. Huang, Y.-C. Liang, and W. Zhang, "Hierarchical passive beamforming for reconfigurable intelligent surface aided communications," *IEEE Wireless Commun. Lett.*, vol. 10, no. 9, pp. 1909–1913, Jun. 2021.
- [12] A. Albanese, F. Devoti, V. Sciancalepore, M. Di Renzo, and X. Costa-Pérez, "MARISA: A self-configuring metasurfaces absorption and reflection solution towards 6G," *arXiv:2112.01949*, Dec. 2021.
- [13] M. Di Renzo, M. Debbah, D.-T.-H. Phan-Huy *et al.*, "Smart radio environments empowered by reconfigurable AI meta-surfaces: an idea whose time has come," *EURASIP Journal on Wireless Communications and Networking*, May 2019.
- [14] K. L. B. H. L. Van Trees and Z. Tian, *Detection Estimation and Modulation Theory, Part I: Detection, Estimation, and Filtering Theory, Detection Estimation and Modulation Theory*. Wiley, 2013.
- [15] W. Tang, M. Z. Chen, X. Chen, J. Y. Dai, Y. Han, M. Di Renzo, Y. Zeng, S. Jin, Q. Cheng, and T. J. Cui, "Wireless communications with reconfigurable intelligent surface: Path loss modeling and experimental measurement," *IEEE Trans. Wireless Commun.*, vol. 20, no. 1, pp. 421–439, Sept. 2021.